Multilevel Converter Control Approach of Active Power Filter for Harmonics Elimination in Electric Grids

Majid Mehrasa[1], Edris Pouresmaeil[2], Mudathir Funsho Akorede[3], Bo Nørregaard Jørgensen[2], João P. S. Catalão[4,5,6,*]

[1] Young Researchers and Elite Club, Sari Branch, Islamic Azad University, Sari, Iran.
[2] Centre for Energy Informatics, University of Southern Denmark, Odense, Denmark.
[3]Department of Electrical & Electronics Engineering, Faculty of Engineering and Technology, University of Ilorin, P.M.B. 1515 Ilorin, Nigeria.
[4] University of Beira Interior, R. Fonte do Lameiro, Covilha, Portugal.
[5] INESC-ID, R. Alves Redol, Lisbon, Portugal.
[6] IST, University of Lisbon, Av. Rovisco Pais, Lisbon, Portugal.

***Abstract*—This paper presents a Direct Lyapunov based control technique for active power filtering in electric grids. The proposed technique through the interfacing system is designed with the goal to compensate the harmonic current components and reactive power provoked by the nonlinear grid-connected loads. In the method, based on multilevel converter topologies, active power in fundamental frequency is injected from the main grid, which results in unity power factor (PF) between grid currents and load voltages. The performance of the proposed control technique in a Shunt Active Power Filter (SAPF) model is validated in both dynamic and steady-state operating conditions. The simulation results show that the proposed scheme can effectively compensate the system background harmonics and improve the performance of the line current harmonics. The main benefit of this approach is that it prevents current overshoot as the proposed model connects to the grid.**

***Index Terms*—Shunt Active Power Filter, Direct Lyapunov Method, Multilevel Converter, Distribution Grid**

I. Nomenclature

Indices

j	1,2
i	a,b,c
K	1,2,3,4

Variables

V_{C_1}, V_{C_2}	dc-voltage of capacitors
V_i	Load voltages
V_d, V_q	Load voltages in the dq frame
i_{dc}	dc-link current
i_{SF_i}	SAPF currents in abc frame
i_{SF_d}, i_{SF_q}	SAPF currents in dq frame
$i^*_{SF_d}, i^*_{SF_q}$	SAPF reference currents in dq frame
$\Delta u_{eq_{dj}}, \Delta u_{eq_{qj}}$	Dynamic part of switching functions
S_{SF}	Nominal power of VSC in SAPF
P_{SF}, Q_{SF}	Active and reactive power of SAPF
$\sum_{n=2}^{\infty} P_{SF_{hn}}$	SAPF injected harmonics in the d-axis
$V(x)$	Lyapunov function

Abbreviations

SAPF	Shunt Active Power Filter
NPC	Neutral Point Clamped
VSC	Voltage Source Converter
HC	Harmonic Curve
CC	Capability Curve
THD	Total Harmonic Distortion

* Corresponding author at: University of Beira Interior, R. Fonte do Lameiro, 6201-001 Covilhã, Portugal. Tel.: +351 275 329914; fax: +351 275 329972.
*E-mail address:*catalao@ubi.pt (J.P.S. Catalão).

$\sum_{n=2}^{\infty} i^*_{SF_{d_{hn}}}, \sum_{n=2}^{\infty} i^*_{SF_{q_{hn}}}$	SAPF total injected harmonics
i_{l_d}, i_{l_q}	Load currents in dq frame
$I_{l_{d1}}, i_{g_{d1}}$	Load and grid currents of main frequency
$I_{SFq_1}, I_{l_{q1}}$	SAPF and load currents of main frequency
$\tilde{I}_{av_d}, \tilde{I}_{av_q}$	Average values of SAPF currents
..	Radius of $i^*_{SF_d}$ versus $i^*_{SF_q}$
$\tilde{\varphi}$	Radius of SAPF HC
$\tilde{\varphi}''$	Radius of SAPF CC
$(-\sim, -\ )$	Center of $i^*_{SF_d}$ versus $i^*_{SF_q}$
$\left(-\tilde{\alpha}, -\tilde{\beta}\right)$	Center of SAPF HC
$\left(-\tilde{\alpha}', -\tilde{\beta}'\right)$	Center of Load HC
$\left(-\tilde{\alpha}'', -\tilde{\beta}''\right)$	Center of SAPF CC
u_{eq_d}, u_{eq_q}	Switching state functions of model
$u^*_{eq_d}, u^*_{eq_q}$	Switching state functions in steady state
S_i	Switching of transistors in each leg
$\sum_{n=2}^{\infty} P_{l_{max\,hn}}$	Maximum active power of the loads in harmonic frequencies
$\sum_{n=2}^{\infty} Q_{l_{max\,hn}}$	Maximum reactive power of loads in harmonic frequencies
PF	Power Factor
DLM	Direct Lyapunov Method
Parameters	
S_R	Stability area of SAPF
S_r	Absorption area of SAPF equilibrium points
V_m	Maximum amplitude of load voltages
V^*_{dc}	dc-link voltage in steady state
I_{dc}	dc-link current in steady state
R'_{SF}	Sum of filter and transformer resistances
L'_{SF}	Sum of filter and transformer inductances
C	Capacity of dc-link
μ	Grid frequency
a_k	Dynamic gains of SAPF

II. Introduction

The rapidly growing use of power electronic-based devices such as thyristor and transistor converters, diode rectifiers, arc furnaces, electric variable speed drives, etc, which draw nonlinear currents from the main source in many industrial companies over the recent years has resulted in generation of large amount of harmonic currents in electric power grid [1-3]. Harmonics generated by these devices not only cause malfunction in the operation of other linear appliances, which increase the total losses in the electric network but also produce unwanted disturbance to the communication network, more voltage and/or current stress, etc. [4].

To tackle this problem, different mitigation strategies have been proposed in the literature. Such solution approaches include selective harmonics elimination control technique based on pole-zero cancelation in load transform function [5], feedback linearization theory and pole placement strategy for harmonic compensation [6], and optimal control technique in *abc* frame for harmonics elimination and power quality improvement during connection of nonlinear and

unbalanced loads to the grid [7] were found to decrease the negative impacts of these frequencies on the utility grid.

Several other strategies in the Active Power Filter (APF) technology for compensation of harmonic current components of nonlinear loads in power network have been proposed. For instance, a multi-loop error generator in dynamic state condition combined with a dc voltage tracking control loop for harmonics filtering in the power grids is proposed in [8]. The performance of the technique was compared with APF and passive filter in the study. Similarly, some predictive and adaptive control techniques based on the behaviour of the system are proposed [9] for fast estimation and tracking of the reference current components in the control loop of APF. Two ANN-based controllers are used in the approach.

Generally, voltage source converter (VSC) is considered as the heart of the interfacing system in APF technology in high-power system multilevel converters. It is a good trade-off solution between performance and cost. The main advantages of multilevel converters are reduced voltage ratings for the switches, good harmonic spectrum which makes possible the use of smaller and less expensive filters, and fast dynamic response in tracking the reference values [10]-[12]. However, the complexity of the control method is increased in this topology. Other control techniques of multilevel converter topologies in APF application, proposed in the literature include [13] and [14].

In [15], a control technique based on the direct current space vector technique for Neutral Point Clamped (NPC) VSC is proposed. The main objective of the technique is to inject harmonic current components and compensation of the reactive power in the fundamental frequency to fix a unity power factor (PF) of the main grid. Our previous work [16] proposed a control technique based on instantaneous active and reactive current for NPC as an interfacing system in the APF. The proposed control technique guarantees injection of a sinusoidal current from the main grid that is in phase with the load voltage during the connection of nonlinear loads to the grid. Also, ref [17] proposed a general control technique of multilevel converter topologies for integration of renewable energy resources to the grid. In other words, this control technique makes possible the connection of any type of renewable energy resources to the grid via a multilevel converter. It also supplies the harmonic currents of nonlinear grid-connected loads.

Of different control techniques in APF applications, Direct Lyapunov Method (DLM) can guarantee an asymptotic stability for system which leads the system variables to their reference values in both dynamic and steady state operating conditions [18]-[20]. In this paper, a control

strategy based on DLM is presented for control of NPC voltage source converter in a Shunt Active Power Filter (SAPF) application. The proposed control technique can guarantee injection of harmonic current components, and compensate the reactive power of the grid-connected load in both dynamic and steady state operating conditions. The performance of the proposed control technique is validated through simulation results using Matlab/Simulink in both transient and steady state operating conditions.

III. The Proposed Model

Figure 1 shows the general schematic diagram of the SAPF, connected to the grid via a three phase Δ/Y transformer. An NPC voltage source converter is the heart of the interfacing system between the energy source and electric grid. It can inject harmonic current components from the source to the grid to supply the harmonic current frequencies of the grid-connected loads. In this study, a three phase diode bridge rectifier with a resistive load is considered as nonlinear load which continuously draws harmonic currents from the utility grid.

A. Dynamic model of SAPF

To design the appropriate control technique for the interfacing system, the dynamic model of the proposed SAPF should first be evaluated. By applying the Kirchhoff's voltage and current laws to the ac and dc sides of the interfacing system in Fig.1, three differential equations in the stationary reference frame can be expressed as presented in eq. (1).

$$\begin{cases} L_{SF}^{'}\dfrac{di_{SF_i}}{dt}+R_{SF}^{'}i_{SF_i}+\left(S_{i_1}-\dfrac{1}{3}\sum_{n=a}^{b,c}S_{n_1}\right)V_{C_1}+\left(S_{i_2}-\dfrac{1}{3}\sum_{n=a}^{b,c}S_{n_2}\right)V_{C_2}-V_i=0 \\ C\dfrac{dV_{C_1}}{dt}-\left(S_{a_1}i_{SF_a}+S_{b_1}i_{SF_b}+S_{c_1}i_{SF_c}\right)+i_{dc}=0 \\ C\dfrac{dV_{C_2}}{dt}+\left(\left(1-S_{a_2}\right)i_{SF_a}+\left(1-S_{b_2}\right)i_{SF_b}+\left(1-S_{c_2}\right)i_{SF_c}\right)+i_{dc}=0 \end{cases} \quad (1)$$

From eq. (1), the equivalent switching state functions of the interfacing system can be obtained as,

$$\begin{cases} u_{eq_{i1}} = \left(S_{i_1} - \frac{1}{3}\sum_{n=a}^{b,c} S_{n_1} \right) \\ u_{eq_{i2}} = \left(S_{i_2} - \frac{1}{3}\sum_{n=a}^{b,c} S_{n_2} \right) \end{cases} \quad (2)$$

Substituting eq. (2) in eq. (1), and using the Park transformation matrix, the general state space equations of the model, obtained in the *dq* reference frame, are presented in eqs. (3) to (6).

$$L_{SF}^{'} \frac{di_{SF_d}}{dt} + R_{SF}^{'} i_{SF_d} - \mu L_{SF}^{'} i_{SF_q} + u_{eq_{d1}} V_{c_1} + u_{eq_{d2}} V_{c_2} - V_d = 0 \quad (3)$$

$$L_{SF}^{'} \frac{di_{SF_q}}{dt} + R_{SF}^{'} i_{SF_q} + \mu L_{SF}^{'} i_{SF_d} + u_{eq_{q1}} V_{c_1} + u_{eq_{q2}} V_{c_2} - V_q = 0 \quad (4)$$

$$C \frac{dV_{c_1}}{dt} - u_{eq_{d1}} i_{SF_d} - u_{eq_{q1}} i_{SF_q} + i_{dc} = 0 \quad (5)$$

$$C \frac{dV_{c_2}}{dt} - u_{eq_{d2}} i_{SF_d} - u_{eq_{q2}} i_{SF_q} + i_{dc} = 0 \quad (6)$$

B. Harmonic compensation capability of SAPF

To design an efficient control technique for the interfacing system, there is a need to evaluate the capability of the SAPF in the injection of harmonic current components into the system. The assumption here is that the reference voltage vector is considered in the direction of *d-axis* vector to fix a stable voltage for the grid and load, thereby making *q-axis* vector of the load voltage zero ($V_q = 0$). In addition, the proposed model should inject the total harmonic current components of load. In other words,

$$i_{SF_d} = i_{SF_d}^{*}, \quad i_{SF_q} = i_{SF_q}^{*} \quad (7)$$

Similarly, the dc link voltage values and equivalent switching state functions of interfacing system in the steady state condition can be expressed as,

$$\begin{cases} V_{c_1} = V_{c_2} = V_{dc}^* \\ u_{eq_{d1}} = u_{eq_{d2}} = u_{eq_d}^* \\ u_{eq_{q1}} = u_{eq_{q2}} = u_{eq_q}^* \end{cases} \tag{8}$$

By replacing the steady state conditions in equations (3) - (6), new state-space equations for the proposed model are obtained as follows:

$$L_{SF}^{'} \frac{di_{SF_d}^*}{dt} + R_{SF}^{'} i_{SF_d}^* - \mu L_{SF}^{'} i_{SF_q}^* + u_{eq_d}^* V_{dc}^* + u_{eq_d}^* V_{dc}^* - V_m = 0 \tag{9}$$

$$L_{SF}^{'} \frac{di_{SF_q}^*}{dt} + R_{SF}^{'} i_{SF_q}^* + \mu L_{SF}^{'} i_{SF_d}^* + u_{eq_q}^* V_{dc}^* + u_{eq_q}^* V_{dc}^* = 0 \tag{10}$$

$$u_{eq_d}^* i_{SF_d}^* + u_{eq_q}^* i_{SF_q}^* - I_{dc} = 0 \tag{11}$$

From eqs. (9) and (10), a set of switching state functions of the model in the steady-state condition can be achieved as,

$$u_{eq_d}^* = \frac{-R_{SF}^{'}}{2V_{dc}^*} \left(\frac{L_{SF}^{'}}{R_{SF}^{'}} \frac{di_{SF_d}^*}{dt} + i_{SF_d}^* - \frac{\mu L_{SF}^{'}}{R_{SF}^{'}} i_{SF_q}^* - \frac{V_m}{R_{SF}^{'}} \right) \tag{12}$$

$$u_{eq_q}^* = \frac{-R_{SF}^{'}}{2V_{dc}^*} \left(\frac{L_{SF}^{'}}{R_{SF}^{'}} \frac{di_{SF_q}^*}{dt} + i_{SF_q}^* + \frac{\mu L_{SF}^{'}}{R_{SF}^{'}} i_{SF_d}^* \right) \tag{13}$$

The average values of instantaneous variations in the reference current components in the control loop of SAPF are defined as given in eq. (14).

$$\frac{di_{SF_d}^*}{dt} = \tilde{I}_{av_d}, \quad \frac{di_{SF_q}^*}{dt} = \tilde{I}_{av_q} \tag{14}$$

If eqs. (12), (13) and (14) are substituted in (11); the general state space model of the SAPF is obtained as eq. (15), which can further be simplified as eq. (16).

$$R_{SF}^{'} i_{SF_d}^{*2} + R_{SF}^{'} i_{SF_q}^{*2} + \left(\tilde{I}_{av_d} L_{SF}^{'} - V_m \right) i_{SF_d}^* + \tilde{I}_{av_q} L_{SF}^{'} i_{SF_q}^* + 2V_{dc}^* I_{dc} = 0 \tag{15}$$

$$\left(i^{*}_{SF_d}+\frac{\tilde{I}_{av_d}L^{'}_{SF}-V_m}{2R^{'}_{SF}}\right)^2+\left(i^{*}_{SF_q}+\frac{L^{'}_{SF}\tilde{I}_{av_q}}{2R^{'}_{SF}}\right)^2=\frac{\left(\tilde{I}_{av_d}L^{'}_{SF}-V_m\right)^2+\tilde{I}^2_{av_q}L^{'2}_{SF}-8R^{'}_{SF}V^{*}_{dc}I_{dc}}{4R^{'2}_{SF}} \tag{16}$$

Looking critically at eq. (16), it is observed that it resembles the general form of equation of a circle, which can be simplified as,

$$\left(i^{*}_{SF_d}+\sim\right)^2+\left(i^{*}_{SF_q}+\quad\right)^2=\text{¨}^2 \tag{17}$$

By comparing (16) with (17), ~ and , which are respectively the horizontal and vertical coordinates of the center of the circle, as well as φ, which is the radius of the circle, can be obtained as,

$$\alpha=\frac{\tilde{I}_{av_d}L^{'}_{SF}-V_m}{2R^{'}_{SF}}$$

$$\beta=\frac{L^{'}_{SF}\tilde{I}_{av_q}}{2R^{'}_{SF}}$$

$$\varphi=\sqrt{\frac{\left(\tilde{I}_{av_d}L^{'}_{SF}-V_m\right)^2+\tilde{I}^2_{av_q}L^{'2}_{SF}-8R^{'}_{SF}V^{*}_{dc}I_{dc}}{4R^{'2}_{SF}}}$$

Figure 2 illustrates the general model of a circle mentioned above in (17). It is used to determine the area required for the SAPF to generate dc and alternative current components in the *d* and *q* reference frames.

The aim of DLM is to control the NPC voltage source converter to generate the load alternative current components and achieve a unity PF in the electric grid. Therefore, the reference currents in the control loop of the SAPF can be written as,

$$i^{*}_{SF_d}=\sum_{n=2}^{\infty}i^{*}_{SF_{d_{hn}}} \tag{18}$$

$$i^{*}_{SF_q}=I_{SFq_1}+\sum_{n=2}^{\infty}i^{*}_{SF_{q_{hn}}} \tag{19}$$

By substituting equations (18) and (19) into (17), eq. (20) is obtained as follows,

$$\left(\sum_{n=2}^{\infty}i^{*}_{SF_{d_{hn}}}+\tilde{\alpha}\right)^2+\left(\sum_{n=2}^{\infty}i^{*}_{SF_{q_{hn}}}+\tilde{\beta}\right)^2=\tilde{\varphi}^2 \tag{20}$$

where

$$\tilde{\alpha} = \alpha$$
$$\tilde{\beta} = I_{SFq_1} + \beta$$
$$\tilde{\varphi} = \varphi$$

Equation (20) is again the general equation of a circle with center $\left(-\tilde{\alpha}, -\tilde{\beta}\right)$ and radius of $\tilde{\varphi}$ as depicted in Fig. 3, called Harmonic Curve (HC) in the SAPF. This curve shows the capability of the SAPF in compensating the nonlinear load harmonic current components. As it can be seen in Fig. 4, SAPF can supply the harmonic currents required in a typical load.

For a proper and efficient operation of the SAPF in eq. (20), the harmonic current components in the *d-axis* should fulfil the condition in (21).

$$\sum_{n=2}^{\infty} i^*_{SF_{d_{hn}}} = \sqrt{\tilde{\varphi}^2 - \left(i_{l_q} + \tilde{\beta} - I_{SF_{q1}}\right)^2} - \tilde{\alpha} \tag{21}$$

The total injected harmonic current components from the SAPF to the load is guided by the equation of the load curve, which is expressed as,

$$\left(i_{l_d} + \tilde{\alpha}'\right)^2 + \left(i_{l_q} + \tilde{\beta}'\right)^2 = \tilde{\varphi}^2$$

(22)

where

$$\tilde{\alpha}' = \tilde{\alpha} - I_{l_{d1}}$$
$$\tilde{\beta}' = \tilde{\beta} - I_{l_{q1}}$$

Fig. 5 compares the proposed SAPF curves and that of the load. As can be seen from this figure, if $\tilde{\alpha}' \to \alpha - i_{g_{d1}}$ and $\tilde{\beta}' \to \beta$ which are obtained from the $I_{l_{d1}} \to i_{g_{d1}}$ and $I_{l_{q1}} \to I_{SF_{q1}}$, the capability of the SAPF in supplying the load current is increased. Given this, only the active power in the fundamental frequency is injected from the main grid to the load and the rest of the currents – the

harmonic current components of load current in *d-axis* and the total load current components in the *q-axis* – are supplied by the SAPF.

C. Active and Reactive power of SAPF

The region of active and reactive power generated by the SAPF in the steady state should be determined in order to validate the maximum capacity of the SAPF in terms of harmonic injection.

Considering $I_{out_{SF}} = i_{SF_d} + ji_{SF_q}$, $V_{out_{SF}} = V_d + jV_q$ and S_{SF} as output current, voltage and power of the SAPF respectively, the injected active and reactive power from the SAPF can be obtained as:

$$S_{SF} = V^*_{out_{SF}} I_{out_{SF}} = P_{SF} + jQ_{SF} \tag{23}$$

Applying the steady state conditions to (23), the injected active and reactive power from the SAPF to the grid in the steady state can be expressed as,

$$P_{SF} = V_m i^*_{SF_d} \tag{24}$$

$$Q_{SF} = -V_m i^*_{SF_q} \tag{25}$$

By putting equations (24) and (25) into (17), eq. (26) is obtained.

$$\left(P_{SF} + \sim V_m\right)^2 + \left(Q_{SF} - \ V_m\right)^2 = \left(\ddot{} V_m\right)^2 \tag{26}$$

Considering the objective of DML control technique, (26) can be rewritten as,

$$\left(\sum_{n=2}^{\infty} P_{SF_{hn}} + \tilde{\alpha}''\right)^2 + \left(Q_{SF} + \tilde{\beta}''\right)^2 = \tilde{\varphi}''^2 \tag{27}$$

where

$$\tilde{\alpha}'' = \alpha V_m$$
$$\tilde{\beta}'' = -\beta V_m$$
$$\tilde{\varphi}'' = \varphi V_m$$

Equation (27) is the equation of a circle with radius of $\tilde{\varphi}''$ and center of $\left(-\tilde{\alpha}'',-\tilde{\beta}''\right)$ which is determined in Fig. 6, and called Capability Curve (CC) in the SAPF. It should be added that CC validates the capability of the SAPF in supplying the load harmonic current components and achieving unity PF by injecting reactive power in the fundamental frequency into the electric grid. The areas that can be supported by the SAPF are determined in Fig. 6.

IV. Dynamic-State Evaluation of SAPF

The unexpected and sudden changes in the load and model parameters lead to some problems in current control loop of the SAPF. In this section, the impacts of the undesired changes are studied through the dynamic state analysis of the proposed model for the design of the appropriate control technique.

A. Direct Lyapunov Method (DLM)

Three different descriptions which are related to the stability of SAPF are shown in Fig. 7. From the figure, DLM leads to asymptotic stability of the system with each initial state during dynamic changes (curve 1) to avoid marginal stability (curve 2) and absolute instability (curve 3) of the system. As it can be seen from curve1, the state spaces variables of the SAPF comes close globally to their reference values in the proposed control technique. This method is based on the total energy of system.

Considering *V(x)* as total energy function in the SAPF and the following assumptions,

$$\begin{cases} V\left(0\right)=0 \\ V\left(x\right)>0 \quad \forall x\neq 0 \\ V\left(x\right)\to\infty \; as \left\|x\right\|\to\infty \\ \dot{V}\left(x\right)<0 \quad \forall x\neq 0 \end{cases} \tag{28}$$

where *V(x)* is generally defined as,

$$V\left(x\right)=\frac{1}{2}L_{SF}^{'}x_1^2+\frac{1}{2}L_{SF}^{'}x_2^2+\frac{1}{2}Cx_3^2+\frac{1}{2}Cx_4^2 \tag{29}$$

and,

$$x_1 = i_{SF_d} - i^*_{SF_d} \tag{30}$$

$$x_2 = i_{SF_q} - i^*_{SF_q} \tag{31}$$

$$x_3 = V_{C_1} - V^*_{dc} \tag{32}$$

$$x_4 = V_{C_2} - V^*_{dc} \tag{33}$$

The switching state functions of the interfaced converter in the proposed model are defined as,

$$u_{eq_{d1}} = u^*_{eq_d} + \Delta u_{eq_{d1}} \tag{34}$$

$$u_{eq_{d2}} = u^*_{eq_d} + \Delta u_{eq_{d2}} \tag{35}$$

$$u_{eq_{q1}} = u^*_{eq_q} + \Delta u_{eq_{q1}} \tag{36}$$

$$u_{eq_{q2}} = u^*_{eq_q} + \Delta u_{eq_{q2}} \tag{37}$$

Taking into account the assumptions in (28) and the general equation of (29), eq. (38) is obtained as,

$$\dot{V}\left(x\right) = L'_{SF}\dot{x}_1 x_1 + L'_{SF}\dot{x}_2 x_2 + C\dot{x}_3 x_3 + C\dot{x}_4 x_4 < 0 \tag{38}$$

Considering equations (3)-(6) and (30)-(33), different parts in (38) can be calculated separately as,

$$\begin{aligned} &L'_{SF}\dot{x}_1 x_1 = -R'_{SF} i^2_{SF_d} + R'_{SF} i_{SF_d} i^*_{SF_d} + \omega L'_{SF} i_{SF_q} i_{SF_d} - \omega L'_{SF} i_{SF_q} i^*_{SF_d} \\ &-u_{eq_{d1}} V_{c_1}\left(i_{SF_d} - i^*_{SF_d}\right) - u_{eq_{d2}} V_{c_2}\left(i_{SF_d} - i^*_{SF_d}\right) + V_d\left(i_{SF_d} - i^*_{SF_d}\right) - \tilde{I}_{av_d}\left(i_{SF_d} - i^*_{SF_d}\right) \end{aligned} \tag{39}$$

$$\begin{aligned} &L'_{SF}\dot{x}_2 x_2 = -R'_{SF} i^2_{SF_q} + R'_{SF} i_{SF_q} i^*_{SF_q} - \omega L'_{SF} i_{SF_d} i_{SF_q} + \omega L'_{SF} i_{SF_d} i^*_{SF_q} \\ &-u_{eq_{q1}} V_{c_1}\left(i_{SF_q} - i^*_{SF_q}\right) - u_{eq_{q2}} V_{c_2}\left(i_{SF_q} - i^*_{SF_q}\right) + V_q\left(i_{SF_q} - i^*_{SF_q}\right) - \tilde{I}_{av_q}\left(i_{SF_q} - i^*_{SF_q}\right) \end{aligned} \tag{40}$$

$$C\dot{x}_3 x_3 = u^*_{eq_d} i_{SF_d}\left(V_{C_1} - V^*_{dc}\right) + u^*_{eq_q} i_{SF_q}\left(V_{C_1} - V^*_{dc}\right) + \Delta u_{eq_{d1}}\left(V_{C_1} i_{SF_d} - i_{SF_d} V^*_{dc}\right) + \Delta u_{eq_{q1}}\left(V_{C_1} i_{SF_q} - i_{SF_q} V^*_{dc}\right) \quad (41)$$

$$C\dot{x}_4 x_4 = u^*_{eq_d} i_{SF_d}\left(V_{C_2} - V^*_{dc}\right) + u^*_{eq_q} i_{SF_q}\left(V_{C_2} - V^*_{dc}\right) + \Delta u_{eq_{d2}}\left(V_{C_2} i_{SF_d} - i_{SF_d} V^*_{dc}\right) + \Delta u_{eq_{q2}}\left(V_{C_2} i_{SF_q} - i_{SF_q} V^*_{dc}\right) \quad (42)$$

Substituting (39)-(42) in (38), eq. (43) is achieved.

$$\begin{aligned}\dot{V}\left(x\right) = &-R'_{SF} i^2_{SF_d} - R'_{SF} i^2_{SF_q} - \frac{R'_{SF}}{2V^*_{dc}}\left(V_{C_1} + V_{C_2}\right) i^{*2}_{SF_d} - \frac{R'_{SF}}{2V^*_{dc}}\left(V_{C_1} + V_{C_2}\right) i^{*2}_{SF_q} - \Delta u_{eq_{d1}}\left(V^*_{dc} i_{SF_d} - V_{C_1} i^*_{SF_d}\right) - \\ &\Delta u_{eq_{d2}}\left(V^*_{dc} i_{SF_d} - V_{C_2} i^*_{SF_d}\right) - \Delta u_{eq_{q1}}\left(V^*_{dc} i_{SF_q} - V_{C_1} i^*_{SF_q}\right) - \Delta u_{eq_{q2}}\left(V^*_{dc} i_{SF_q} - V_{C_2} i^*_{SF_q}\right)\end{aligned} \quad (43)$$

If the capacitor voltage on the dc side of the interfacing system is tuned to the reference values ($V_{C_1} + V_{C_2} \to 2V^*_{dc}$), the proposed control technique works efficiently during harmonic currents injection.

Equations (44)-(47) demonstrate the equivalent switching functions of the dynamic section in the SAPF which make the control loop have a robust reaction against undesirable disturbances.

$$\Delta u_{eq_{d1}} = a_1\left(V^*_{dc} i_{SF_d} - V_{C_1} i^*_{SF_d}\right) \quad (44)$$

$$\Delta u_{eq_{d2}} = a_2\left(V^*_{dc} i_{SF_d} - V_{C_2} i^*_{SF_d}\right) \quad (45)$$

$$\Delta u_{eq_{q1}} = a_3\left(V^*_{dc} i_{SF_q} - V_{C_1} i^*_{SF_q}\right) \quad (46)$$

$$\Delta u_{eq_{q2}} = a_4\left(V^*_{dc} i_{SF_q} - V_{C_2} i^*_{SF_q}\right) \quad (47)$$

B. Impact of coefficient values

The changes in the values of a_i in the proposed SAPF noticeably impact on the THD of the grid currents, the grid PF, as well as the dynamic response of DLM during the transient period. The impacts of coefficient variations can be surveyed through the inherent frequencies in the close loop control of the SAPF.

Based on the definition in (30)-(33) and with reference to eqs. (3)-(6), a new set of dynamic equations for the proposed model are achieved as,

$$L_{SF}^{'}\frac{dx_1}{dt}+R_{SF}^{'}x_1-\mu L_{SF}^{'}x_2+u_{eq_{d1}}x_3+u_{eq_{d2}}x_4+\Delta u_{eq_{d1}}V_{dc}^{*}+\Delta u_{eq_{d2}}V_{dc}^{*}=0 \tag{48}$$

$$L_{SF}^{'}\frac{dx_2}{dt}+R_{SF}^{'}x_2+\mu L_{SF}^{'}x_1+u_{eq_{q1}}x_3+u_{eq_{q2}}x_4+\Delta u_{eq_{q1}}V_{dc}^{*}+\Delta u_{eq_{q2}}V_{dc}^{*}=0 \tag{49}$$

$$C\frac{dx_3}{dt}-u_{eq_{d1}}x_1-u_{eq_{q1}}x_2-u_{eq_{d1}}i_{SF_d}^{*}-u_{eq_{q1}}i_{SF_q}^{*}+i_{dc}=0 \tag{50}$$

$$C\frac{dx_4}{dt}-u_{eq_{d2}}x_1-u_{eq_{q2}}x_2-u_{eq_{d2}}i_{SF_d}^{*}-u_{eq_{q2}}i_{SF_q}^{*}+i_{dc}=0 \tag{51}$$

Substituting (34)-(37) into the (48)-(51), we have,

$$\dot{x}_1=\left(\frac{-R_{SF}^{'}-\lambda_1V_{dc}^{*2}-\lambda_2V_{dc}^{*2}}{L_{SF}^{'}}\right)x_1+\left(\omega\right)x_2+\left(\frac{\lambda_1i_{SF_d}^{*}V_{dc}^{*}-u_{eq_d}^{*}}{L_{SF}^{'}}\right)x_3+\left(\frac{\lambda_2i_{SF_d}^{*}V_{dc}^{*}-u_{eq_d}^{*}}{L_{SF}^{'}}\right)x_4 \tag{52}$$

$$\dot{x}_2=-\left(\omega\right)x_1+\left(\frac{-R_{SF}^{'}-\lambda_3V_{dc}^{*2}-\lambda_4V_{dc}^{*2}}{L_{SF}^{'}}\right)x_2+\left(\frac{\lambda_3i_{SF_q}^{*}V_{dc}^{*}-u_{eq_q}^{*}}{L_{SF}^{'}}\right)x_3+\left(\frac{\lambda_4i_{SF_q}^{*}V_{dc}^{*}-u_{eq_q}^{*}}{L_{SF}^{'}}\right)x_4 \tag{53}$$

$$\dot{x}_3=\left(\frac{\lambda_1V_{dc}^{*}i_{SF_d}^{*}+u_{eq_d}^{*}}{C}\right)x_1+\left(\frac{\lambda_3V_{dc}^{*}i_{SF_q}^{*}+u_{eq_q}^{*}}{C}\right)x_2-\left(\frac{\lambda_1i_{SF_d}^{*2}+\lambda_3i_{SF_q}^{*2}}{C}\right)x_3+\left(\frac{u_{eq_d}^{*}i_{SF_d}^{*}+u_{eq_q}^{*}i_{SF_q}^{*}-i_{dc}}{C}\right) \tag{54}$$

$$\dot{x}_4=\left(\frac{\lambda_2V_{dc}^{*}i_{SF_d}^{*}+u_{eq_d}^{*}}{C}\right)x_1+\left(\frac{\lambda_4V_{dc}^{*}i_{SF_q}^{*}+u_{eq_q}^{*}}{C}\right)x_2-\left(\frac{\lambda_2i_{SF_d}^{*2}+\lambda_4i_{SF_q}^{*2}}{C}\right)x_4+\left(\frac{u_{eq_d}^{*}i_{SF_d}^{*}+u_{eq_q}^{*}i_{SF_q}^{*}-i_{dc}}{C}\right) \tag{55}$$

Equations (52)-(55) are linearized model around the operating points of the proposed model. From the model, the state matrix of the SAPF in both dynamic and state-space conditions can be obtained as,

$$A=\begin{bmatrix} \frac{-R_{SF}^{'}-a_1V_{dc}^{*2}-a_2V_{dc}^{*2}}{L_{SF}^{'}} & \mu & \frac{a_1i_{SF_d}^{*}V_{dc}^{*}-u_{eq_d}^{*}}{L_{SF}^{'}} & \frac{a_2i_{SF_d}^{*}V_{dc}^{*}-u_{eq_d}^{*}}{L_{SF}^{'}} \\ -\mu & \frac{-R_{SF}^{'}-a_3V_{dc}^{*2}-a_4V_{dc}^{*2}}{L_{SF}^{'}} & \frac{a_3i_{SF_q}^{*}V_{dc}^{*}-u_{eq_q}^{*}}{L_{SF}^{'}} & \frac{a_4i_{SF_q}^{*}V_{dc}^{*}-u_{eq_q}^{*}}{L_{SF}^{'}} \\ \frac{a_1V_{dc}^{*}i_{SF_d}^{*}+u_{eq_d}^{*}}{C} & \frac{a_3V_{dc}^{*}i_{SF_q}^{*}+u_{eq_q}^{*}}{C} & \frac{a_1i_{SF_d}^{*2}+a_3i_{SF_q}^{*2}}{C} & 0 \\ \frac{a_2V_{dc}^{*}i_{SF_d}^{*}+u_{eq_d}^{*}}{C} & \frac{a_4V_{dc}^{*}i_{SF_q}^{*}+u_{eq_q}^{*}}{C} & 0 & -\frac{a_2i_{SF_d}^{*2}+a_4i_{SF_q}^{*2}}{C} \end{bmatrix} \quad (56)$$

The natural frequencies of the state matrix can be used to identify the dynamic response of the SAPF in harmonic currents compensation during connection of nonlinear load to the grid. For instance, if the dynamic gains of the entire model are considered to be 0.0002, the fourth order equation of model can be achieved as,

$$s^4+20026.54s^3+1005\times10^6s^2+13.4\times10^8s+14\times10^6 \quad (57)$$

By imposing zero onto (47), the inherent frequencies of whole system can be obtained as,

$s_1=-0.011,\quad s_2=-1.32,\quad s_3=-10012.61+30078.1i,\quad s_4=-10012.61-30078.1i$.

The real part of these frequencies is located in the left side of the axis and it verifies that the SAPF is globally asymptotically stable in both steady-state and dynamic conditions.

Table I shows the impact of variation in the dynamic gains in the PF between the grid current and load voltage, the THD of the grid current and the dynamic response of DLM after the connection of the SAPF to the grid. As can be seen, THD of the grid current decreases significantly as gain increases and PF between grid current and load voltage approaches unity for the a_i more than 1e-5. Also, the transient response time approaches its minimum values when the gain value increases. Therefore, based on these results, $a_i=1e-4$ and $a_i=1e-3$ can be considered as the best options for the DLM.

V. Simulation Parameters and Results

The general schematic diagram of the SAPF based on DLM is depicted in Fig. 8. It is the Thévenin equivalent model of an electric grid, grid-connected load, interfacing system and control scheme. This model is considered for simulation analyses using the Matlab/ Simulink

toolbox, to validate the capabilities of DLM for the control of NPC VSC during the connection of nonlinear loads to the grid. For this case, the capability of the DLM in the SAPF to inject harmonic current components and active and reactive power sharing between the grid and the load will be investigated.

Initially, a three phase diode bridge rectifier whose resistance is 30 Ω, is connected to the grid to draw nonlinear currents from the utility grid. This scenario is continued until t=0.1 sec; while the SAPF is integrated to the grid. During this step, the capability of DLM in supplying the harmonic current components of nonlinear load will be evaluated and the other capabilities of DLM for control of the interfacing system in the SAPF will be presented. The network parameters, including the rating and impedances of model components for simulation analysis are given in Table II.

A. SAPF connected to the grid

This section examines the dynamic and steady-state responses of the DLM before and after integration of the SAPF into the grid. Fig. 9 shows the load, grid, and SAPF currents before and after SAPF connection to the grid. As can be seen from this figure, the grid initially injected nonlinear current to the load before the SAPF was connected to the grid. However, integration of the SAPF to the grid at t=0.1 sec implies that the harmonic current components have been supplied by the SAPF within a very short transient period and the grid current is rid of harmonic contents. This result validates the capability of the DLM in controlling the interfacing system for injection of harmonic current components during the connection of nonlinear load to the grid.

Figures 10 and 11 show the fundamental and harmonic current components of the load, grid, and SAPF in d-q reference frames before and after connection of SAPF to the utility grid. These figures demonstrate the capability of the DLM in tracking the reference current components based on the objectives of proposed model.

As illustrated in Fig. 10, before connection of the SAPF to the grid, the current components in both fundamental and harmonic frequencies in the *d-axis* are injected by the main grid. But, at t=0.1 sec the SAPF supplies the whole harmonic current frequencies of the load in the *d-axis* and the rest current in the fundamental frequency, which is 14 A, is supplied by the main grid.

The same scenario is repeated for the current components in the *q-axis* before connection of the SAPF to the grid and as shown in Fig. 11, after the connection of SAPF to the grid, the whole load current components in both fundamental and harmonic frequencies in the *q-axis* are injected by the SAPF. Therefore, the injected current from the grid to the load is free of any current components of the q-axis.

Figure 12 shows the active power sharing between the load, grid and SAPF before and after integration of SAPF into the grid. As can be seen, whole the active power of load in both fundamental and harmonic frequencies are supplied by main grid, before the connection of SAPF to the grid. However, after connection of the SAPF, harmonic components are injected by SAPF and only the active power in fundamental frequency is supplied by grid.

Similarly, Figure 13 shows the reactive power sharing between the load, grid and SAPF before and after integration of SAPF into the grid. The same scenario is repeated for reactive power sharing and the reactive power components are supplied by the main grid before the connection of SAPF into the grid. But, after the connection of the SAPF to the main grid, the whole reactive power in fundamental and harmonic frequencies are injected from the SAPF to the grid and main grid is free of any reactive power components.

Figure 14 shows the grid current and load voltage in phase *a* and the power factor between them. As shown in Fig. 14(a) after the connection of SAPF to the grid, load voltage and grid current are in phase and grid current is becomes sinusoidal. This follows that the injected current from the grid to the load is free of harmonic and reactive power. Figure 14(b) shows that the value of the PF between the grid current and load voltage is equal to unity after a transient event on the SAPF-connected grid.

The PF between load voltages and grid currents in the three-phase system before and after the connection of the SAPF are shown in Table III. On the other hand, Table IV shows the comparison between the THD of grid currents in the three phases before and after connection of the SAPF to the grid, which validate the capability of the proposed technique in harmonic current compensation during connection of nonlinear load to the grid.

VI. Conclusion

A control strategy based on direct Lyapunov method (DLM) for multilevel converters, called Shunt Active Power Filter (SAPF), has been proposed in this paper. By setting appropriate reference current in the control loop of the proposed model, all the reactive power of the grid-connected load in both harmonic and fundamental frequencies can be injected via the interfacing system. The performance of the proposed control technique was validated through time domain simulations in Matlab/Simulink. Interestingly, the results obtained revealed that, with the SAPF connected to the grid, current overshoot was avoided. Hence, the proposed control technique can be used as a power quality improvement and power factor correction device in an energy distribution network.

VII. Acknowledgements

This work was supported by FEDER funds (European Union) through COMPETE, and by Portuguese funds through FCT, under Projects FCOMP-01-0124-FEDER-020282 (Ref. PTDC/EEA-EEL/118519/2010) and UID/CEC/50021/2013. Also, the research leading to these results received funding from the EU Seventh Framework Programme FP7/2007–2013 under grant agreement no. 309048.

References

1. Barote, L., Marinescu, C., “Software method for harmonic content evaluation of grid connected converters from distributed power generation systems,” *Energy*, Vol. 66, pp. 401-412, 2014.
2. Singh, G. K. “Power system harmonics research: a survey,” *European Trans on Electric Power*, Vol. 19, No. 2, pp.151-172, 2007.
3. Asiminoaei, L., Rodriguez, P., Blaabjerg, F., and Malinowski, M. “Reduction of switching losses in active power filters with a new generalized discontinuous-PWM strategy,” *IEEE Trans. Ind. Electron*, Vol. 55, No. 1, pp. 467–471, 2008.
4. Pouresmaeil, E., Akorede, MF., and Hojabri, M. “A hybrid algorithm for fast detection and classification of voltage disturbances in electric power systems,” *European Transaction on Electrical Power*, Vol. 21, No. 1, pp.555-564, 2010.

5. Zhou, H., Li, Y. W., Zargari, N. R., Cheng, Z., Ruoshui, N., and Zhang, Y. “Selective Harmonic Compensation (SHC) PWM for Grid-Interfacing High-Power Converters,” *IEEE Trans. Power. Electron*; Vol. 29, No. 3, pp. 1118–1127, 2014.
6. Mendalek, N., AI-Haddad, K., Fnaiech, F., and Dessaint, L. A. “Nonlinear control technique to enhance dynamic performance of a shunt active power filter,” *IEE Proceedings Electric Power Applications*, Vol. 150, No. 4, pp. 373-79, 2003.
7. George, S., and Agarwal, V. “A DSP Based Optimal Algorithm for Shunt Active Filter under Nonsinusoidal Supply and Unbalanced Load Conditions,” *IEEE Trans. Power. Electron*, Vol. 22, No. 2, pp. 593–601, 2007.
8. Sharaf, AM., Wang, W., and Altas, I. H. “A novel hybrid active filter compensator for stabilization of wind-utility grid interface scheme,” *European Transaction on Electrical Power*; Vol. 20, No. 3, pp. 306–326, 2010.
9. Bhattacharya, A., and Chakraborty, C. “A shunt active power filter with enhanced performance using ANN-based predictive and adaptive controllers,” *IEEE Trans. Ind. Electron*, Vol. 58, No. 2, pp. 421–428, 2011.
10. Mirzaei, A., Jusoh, A., Salam, Z. “Design and implementation of high efficiency non-isolated bidirectional zero voltage transition pulse width modulated DC–DC converters,” *Energy*, Vol. 47, No. 1, pp. 358-369, 2012.
11. Dargahi, V., Sadigh, A.K., Pahlavani, M.R.A., Shoulaie, A. “DC (direct current) voltage source reduction in stacked multicell converter based energy systems,” *Energy*, Vol. 46, No. 1, pp. 649-663, 2012.
12. Kangarlu, M.F, Pahlavani, M.R.A. “Cascaded multilevel converter based superconducting magnetic energy storage system for frequency control,” *Energy*, Vol. 70, No. 1, pp. 504–513, 2014.
13. Vodyakho, O., Kim, T., and Kwak, S. “Comparison of the space vector current controls for active power filters,” *Proceedings, Industrial Electronics, IECON 2008. 34th Annual Conference of IEEE*. 2008’ pp. 612–617, *2008*.
14. Pouresmaeil, E., Montesinos-Miracle, D., and Gomis-Bellmunt, O. “Control scheme of three-level NPC inverter for integration of renewable energy resources into AC grid,” *IEEE System Journal, Vol.* 6, No. 2, pp. 242-53, 2012.
15. Vodyakho, O., Hackstein, D., Steimel, A., and Kim, T. “Novel direct current-space-vector control for shunt active power filters based on three-level inverters,” *IEEE Trans. Power. Electron*, Vol. 23, No. 4, pp. 1668–1678, 2008.
16. Pouresmaeil, E., Montesinos-Miracle, D., Gomis-Bellmunt, O., and Sudrià-Andreu, A. “Instantaneous Active and Reactive Current Control Technique of Shunt Active Power Filter Based on the Three-Level NPC Inverter,” *European Trans on Electric Power*, Vol. 21, No. 7, pp. 2007–22, 2011.

17. Pouresmaeil, E., Gomis-Bellmunt, O., Montesinos-Miracle, D., and Bergas-Jané, J. “Multilevel converters control for renewable energy integration to the power grid,” *Energy*, Vol. 36, No. 2, pp. 950–963, 2011.
18. Komurcugil, H., and Kukrer, O. “A new control strategy for single-phase shunt active power filters using a Lyapunov function,” *IEEE Trans. Ind. Electron*, Vo. 53, No. 1, pp. 305–312, 2006.
19. Hua, C. C., Li, C. H., and Lee, C. S. “Control analysis of an active power filter using Lyapunov candidate,” *IET Power Electron*, Vol. 2, No. 4, pp. 325–334, 2008.
20. Rahman,i S., Hamadi, A., Al-Haddad, K. “A Lyapunov-Function-Based Control for a Three-Phase Shunt Hybrid Active Filter,” *IEEE Trans. Ind. Electron*, Vol. 59, No. 3, pp. 1418–1429, 2012.

Figures

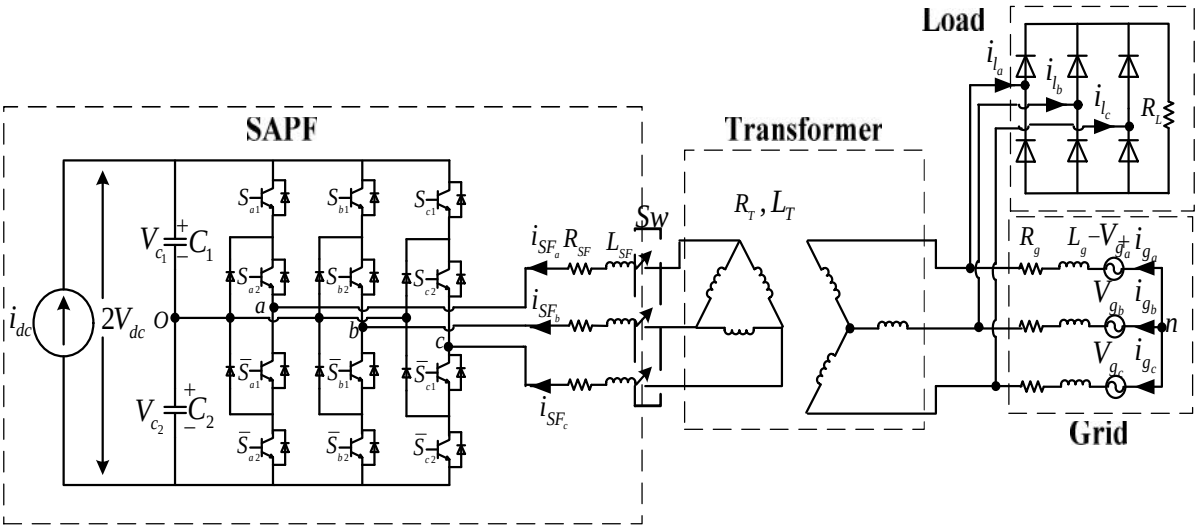

Fig. 1. General schematic diagram of SAPF based on the NPC VSC.

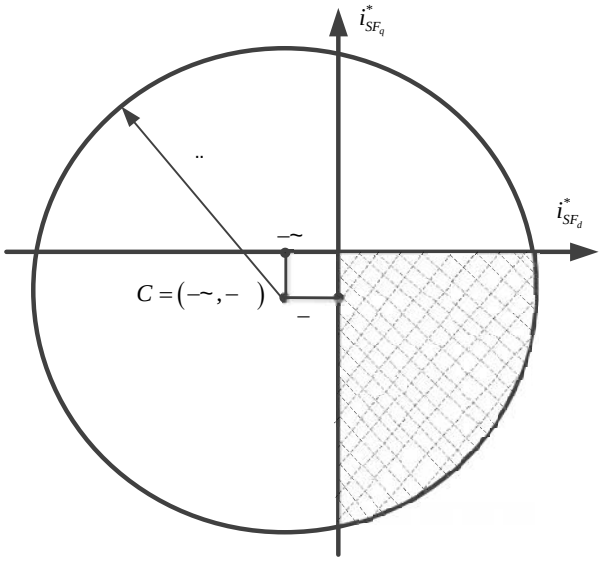

Fig. 2. Reference currents of SAPF in the steady state condition.

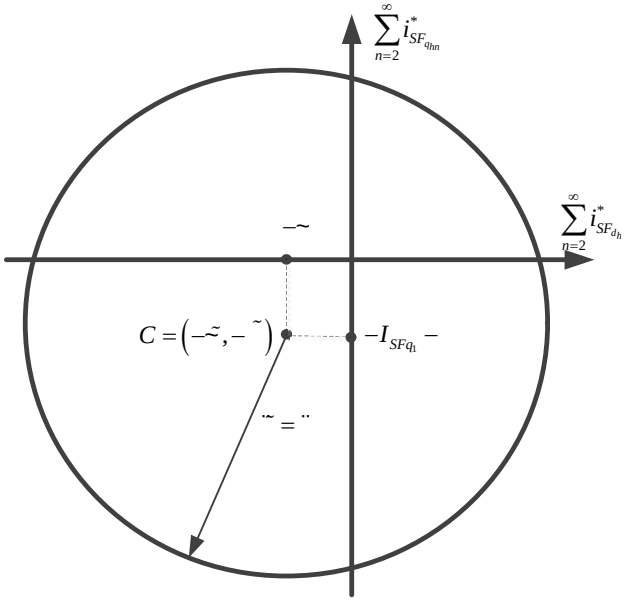

Fig. 3. Harmonic curve in SAPF.

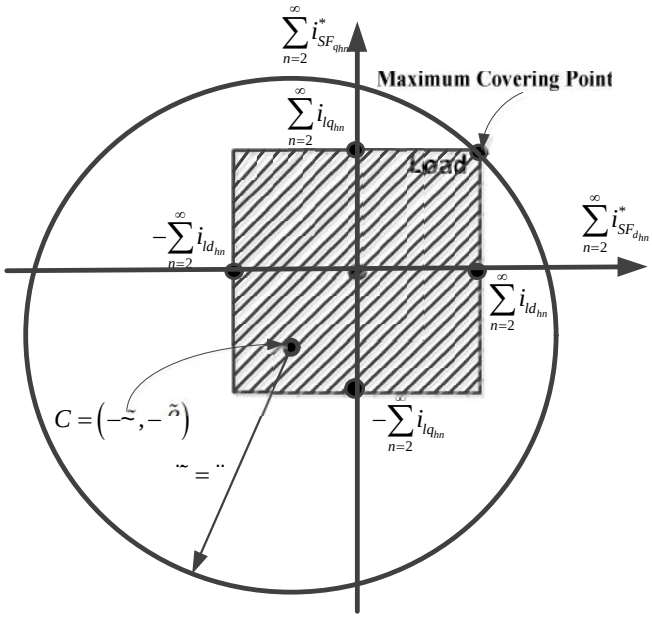

Fig. 4. HC for different loads.

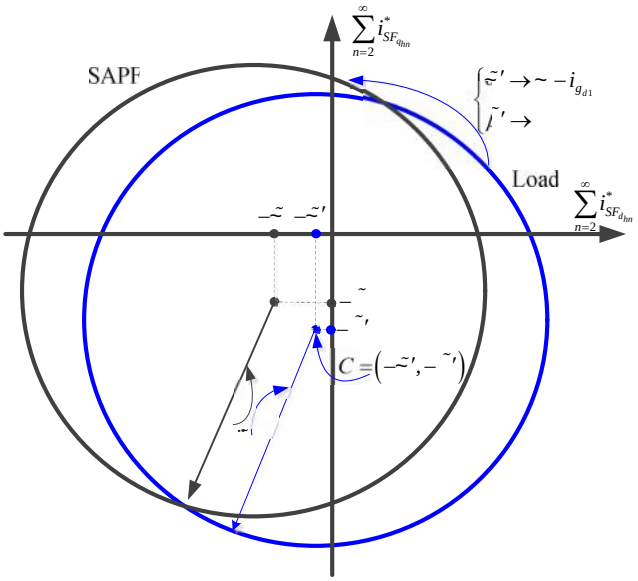

Fig. 5. Comparison of SAPF and load curves.

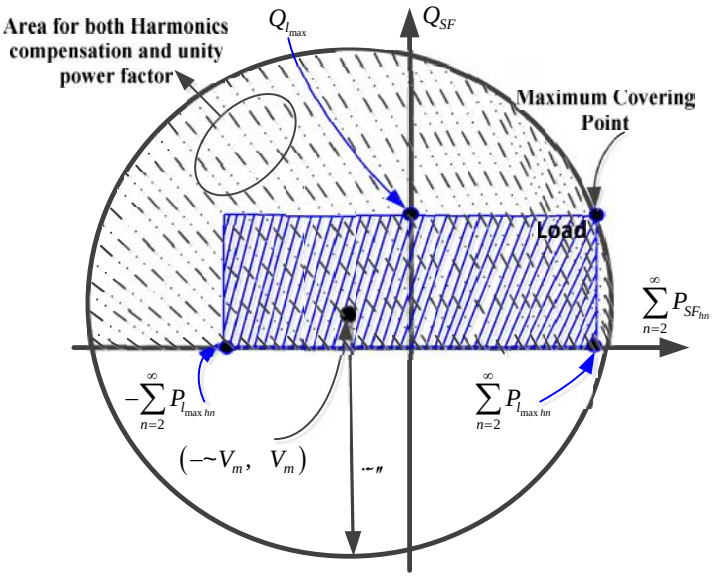

Fig. 6. Capability Curve of SAPF.

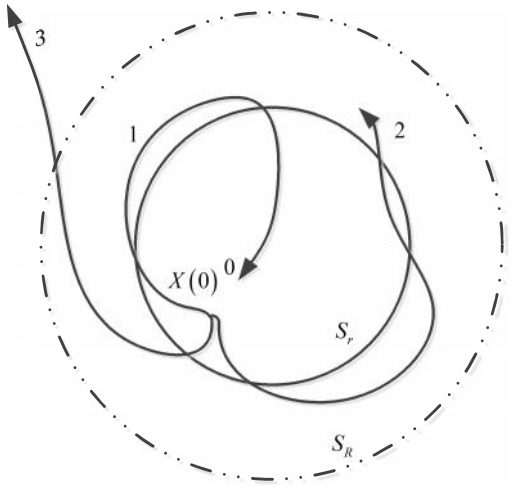

Fig.7. Different stability situations, (1) asymptotically stable, (2) marginally stable, (3) unstable.

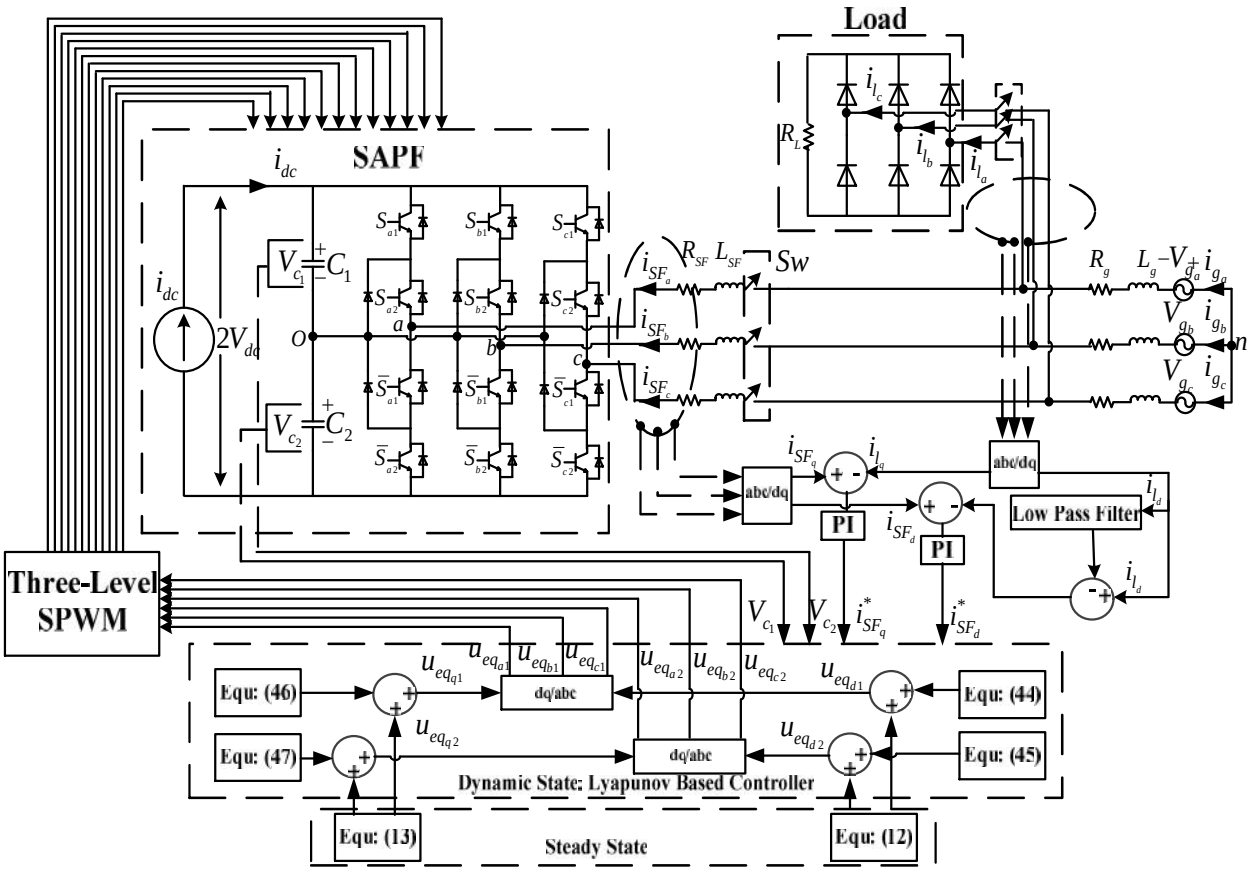

Fig.8. The overall control scheme.

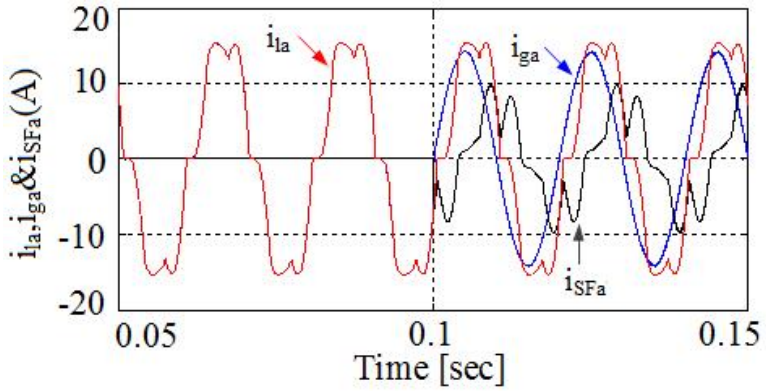

Fig. 9. Load, grid and SAPF currents before and after connection of SAPF to the grid.

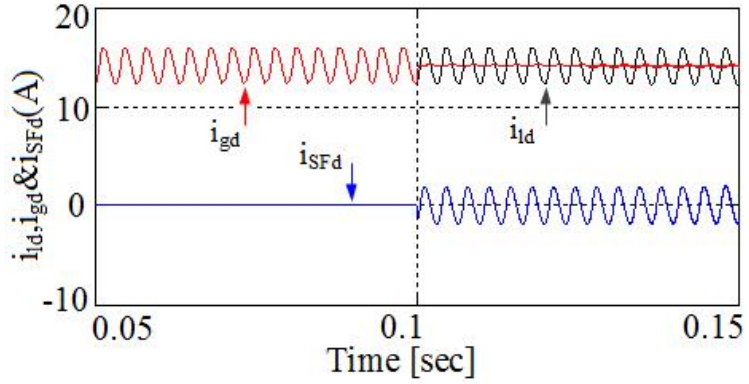

Fig.10. d-axis of load, grid, and SAPF currents in fundamental and harmonic frequencies, before and after connection of SAPF to the grid.

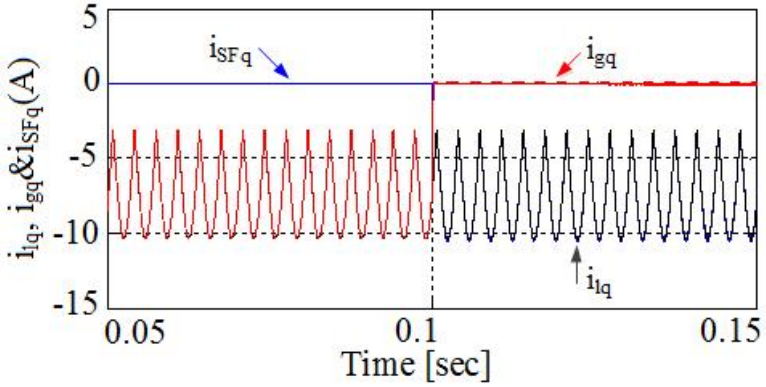

Fig. 11. q-axis of load, grid and SAPF currents in fundamental and harmonic frequencies, before and after connection of SAPF to the grid.

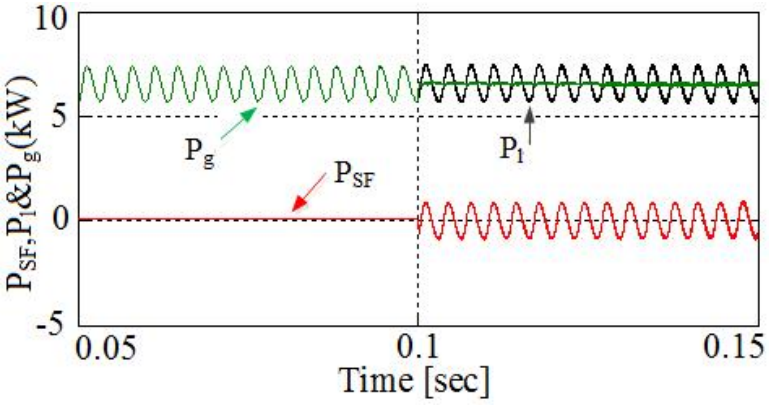

Fig.12. Active power sharing between load, grid and SAPF.

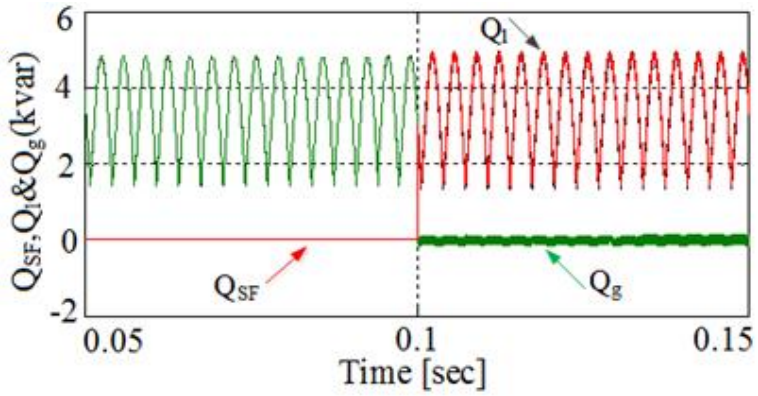

Fig.13. Share of reactive power between load, grid and SAPF.

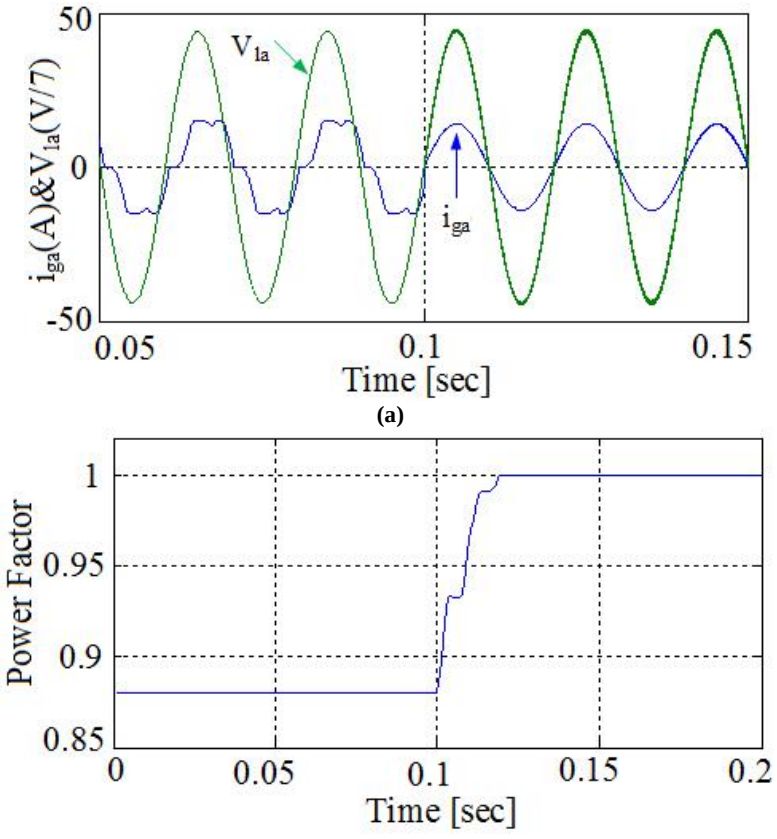

Fig. 14. (a) Load voltage and grid current, (b) PF of grid, before and after connection of SAPF to the grid.

Tables

Table I. Impacts of dynamic gain variations.

a_i	1e-7	1e-6	1e-5	1e-4	1e-3	1e-2	1e-1	1
Power Factor (%)	96.31	97.9	99.98	100	100	100	100	100
THD (%)	62.6	34.2	5.5	0.56	0.58	0.6	0.6	0.6
Transient Response (ms)	eps	eps	60	50	50	45	41	41

Table II. Simulation parameters.

Grid Voltage	380 Vrms
Input Voltage	1000 volt DC
Main Frequency	50 Hz
Inverter Resistance	0.1 Ω
Inverter Inductance	0.45 mH
$¥_1 = a_1$	0.01
$¥_2 = a_2$	0.001
Switching Frequency	10 kHz
SAPF Power Rating	19.5 kVA

Table III. Power Factor analysis.

PF Grid	Before Connection	After Connection
PF1 (%)	88.02	100
PF2 (%)	88.01	100
PF3 (%)	88.01	100

Table IV. THD of the grid currents.

Grid Currents	Before Connection	After Connection
i_{ga} (%)	16.6	0.57
i_{gb} (%)	16.51	0.605
i_{gc} (%)	16.42	0.602